The Handbook of Brain Theory and Neural Networks

EDITED BY
Michael A. Arbib

A Bradford Book
THE MIT PRESS
Cambridge, Massachusetts
London, England

Oscillatory and Bursting Properties of Neurons

Xiao-Jing Wang and John Rinzel

Introduction

Rhythmicity is a common feature of temporal organization in neuronal firing patterns. Historically, when recordings from *isolated* nerves became possible in the 1930s, systematic study of repetitive firing behaviors ensued. Arvanitaki (1939) and Hodgkin (1948) identified three categories of crustacean axons by their rhythmic discharge patterns: those that fire repetitively over a wide (I) or narrow (II) range of frequencies and those whose firing hardly repeats (III). Later, Arvanitaki also pioneered the *Aplysia* preparation and discovered *bursting* oscillations where impulse clusters occur periodically, separated by phases of quiescence.

Since then, many other stereotypical single-neuron patterns, including a fascinating variety of endogeneous oscillations, have been identified (Llinás, 1988; Connors and Gutnick, 1990). One wonders anew about categorizing neuronal firing modes and the criteria on which to base such a classification. Hodgkin and Huxley (1952) showed that many spiking properties can be explained in terms of various active ionic currents across the cell membrane. Today, many types of ion channels are known (see ION CHANNELS: KEYS TO NEURONAL SPECIALIZATION), and some specific neuronal rhythms have been linked to selected subsets of channels. However, membrane potential oscillations with apparently similar characteristics can be generated by different ionic mechanisms and by other biophysical factors, such as cable properties. In addition, a given cell type may display several different firing patterns under different neuromodulatory conditions. For these reasons, the visual appearance of particular voltage time courses and the presence of certain ionic mechanisms are insufficient bases for classification. A rational scheme should consider a cell's complete *repertoire* of dynamical modes and the nature of transitions between modes.

Here we apply the mathematics of dynamical systems to describe precisely the dynamical modes of neuronal firing and the transformations between them. The approach was pioneered by FitzHugh with his phase space analysis of nerve membrane excitability (FitzHugh, 1961). In this theoretical framework, membrane dynamics is described by coupled *differential equations*, e.g., à la Hodgkin and Huxley (cf. Rinzel and Ermentrout, 1989), the behavior modes by *attractors*, and the transitions between modes by *bifurcations*. The rest state is represented by a time-independent *steady state* and repetitive firing by a *limit cycle*. The transition from resting to oscillating typically occurs either through a *Hopf bifurcation* or a *homoclinic bifurcation* (Figure 1); (e.g., see Rinzel and Ermentrout, 1989; and DYNAMICS AND BIFURCATION OF NEURAL NETWORKS). The firing frequency versus applied current curves are qualitatively different in the two cases (minimum frequency being non-zero or zero, respectively), and they might subserve an abstract basis

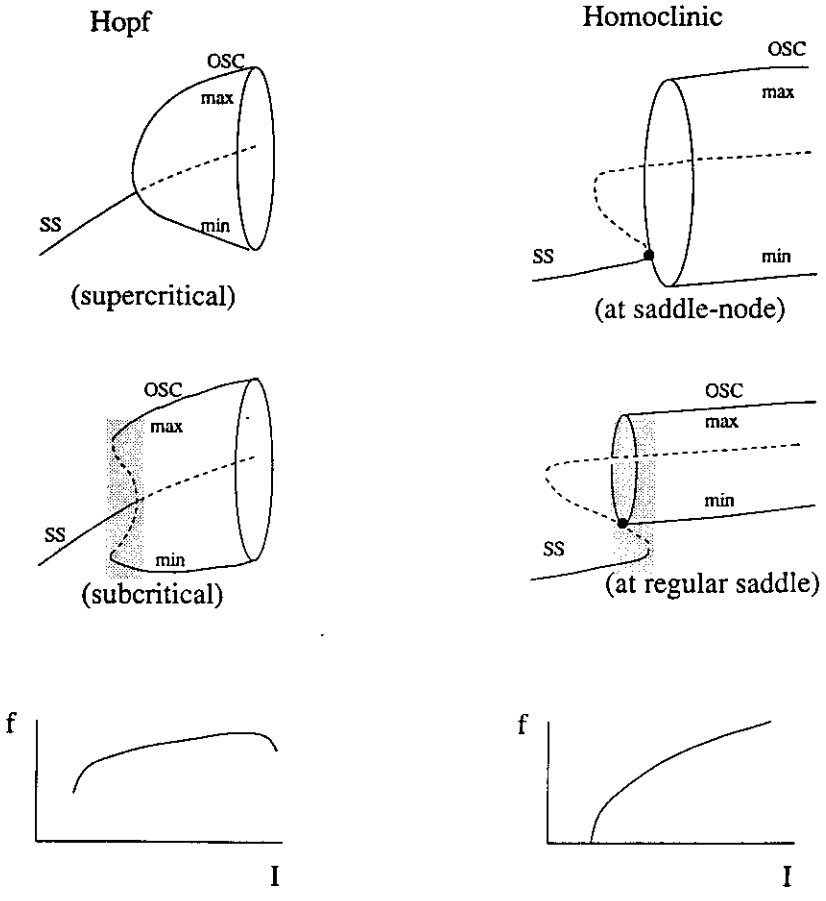

Figure 1. Schematic bifurcation diagrams from a steady state (SS) to an oscillatory firing state (OSC). The abscissa is a control parameter such as the applied current intensity. The ordinate corresponds to the membrane potential, the repetitive firing state being indicated by the maximal (max) and minimal (min) amplitudes of the oscillatory membrane potential. The solid curve indicates stable and the dashed curve unstable. In the lowermost panels, the ordinate (f) is the frequency of repetitive firing and I is applied current. The left panels show Hopf bifurcation. At the onset of oscillation, the rhythmic amplitude is small and the frequency is finite. The bifurcation may be supercritical, where the new oscillatory branch is stable; or subcritical, where the new oscillatory branch is unstable and becomes stable at a turning point. The right panels show homoclinic bifurcation. It corresponds to the coalescence of an oscillatory state with an unstable steady state. This steady state can be either of saddle-node or saddle type. As this bifurcation point is approached, the amplitude of oscillation remains finite, while the rhythmic frequency tends to zero (the period diverging to infinity). In the case of a subcritical Hopf bifurcation or a normal homoclinic bifurcation, there is a range of parameter values where a steady-state attractor and an oscillatory attractor coexist (bistability, shaded region).

for the distinction between the Arvanitaki-Hodgkin type II and type I axons. Our review generalizes this theoretical methodology to characterize various *bursting* oscillations in single neurons, elaborating on a qualitative classification scheme for bursting mechanisms proposed by Rinzel (1987).

Neuronal Bursting: Examples

We summarize some qualitative features of observed bursting patterns and then relate these to our classification scheme. We briefly mention conductance mechanisms that are *sufficient* to produce some of these bursting oscillations. While network synaptic interactions and dendritic cable properties influence bursting behavior, for the most part, our discussion concerns an isolated, isopotential neuron. The main biophysical idea is that rhythmicity is generated by a depolarization process which is autocatalytic (positive feedback), followed by a *slower* repolarization process (negative feedback). These opposing processes may involve activation and slow inactivation of an inward ionic current or a fast inward current and a slower outward current. Such features underlie action potential generation, and for bursting, there is at least another *slower* negative feedback process.

The burst pattern shown in Figure 2*A* has a *square-wave* form, with abrupt periodic switching between rest (silent phase) and depolarized repetitive firing (active phase). Spiking here is primarily caused by a *high-threshold* fast calcium current and a Hodgkin-Huxley-like potassium current. A minimal biophysical mechanism for square-wave bursting involves a calcium-activated potassium current (see Rinzel, 1985, and citation there for Chay and Keizer, 1983). During the active phase, each calcium spike increases slightly $[Ca^{2+}]_i$, slowly turning on this current and eventually repolarizing the membrane to terminate the active phase. During the silent phase, the Ca^{2+} channels are closed, $[Ca^{2+}]_i$ decreases, and as the potassium conductance deactivates, the cell slowly depolarizes until the threshold for the next active phase is reached. Suggested alternative mechanisms for this type of bursting include slow inactivation by Ca^{2+}, and/or by voltage of the Ca^{2+} current (Cook, 1991). Here, if spikes are abolished by pharmacologically blocking the calcium current, bursting is lost.

While the dopamine-secreting neuron (Figure 2*B*) superficially appears to be a square-wave burster, we would not classify it as such. Its underlying slow wave persists even when action potentials are blocked. It appears to be of dendritic origin, and it drives somatic spiking through electrotonic interaction.

The bursting patterns of Figure 2*C* and 2*D* exhibit brief spike bursts riding on a slow *triangular wave*. Thalamocortical relay cells (see Figure 2*C*) burst at the delta-wave frequency (3 Hz) of quiet sleep (Steriade, McCormick, and Sejnowski, 1993), while the 5-Hz oscillation in inferior olivary cells (see Figure 2*D*) is probably involved with movement tremor (see Llinás and Yarom, 1986). Remarkably, in both cases, rhythmic bursting occurs for maintained hyperpolarizing rather than depolarizing stimuli. The underlying slow wave (as a result of a low-threshold calcium current) is unmasked when the fast action potentials are blocked and is sometimes seen for modest hyperpolarizing inputs, even without blocking spikes. The Ca^{2+} current activates rapidly below the voltage threshold for action potentials. Its inactivation by voltage, with a time scale like that of the triangular wave's depolarization, provides the slow negative feedback.

The *Aplysia* R15 neuron is the quintessential experimental model of an endogenous burster (Figure 2*E*) (Adams and Benson, 1985). The sodium spike rate during a burst first increases and then decreases; hence, the term *parabolic* bursting. Blocking these spikes reveals an underlying quasi-sinusoidal slow wave that is generated primarily by a Ca^{2+} current. This current activates more slowly and at lower depolarizations than that associated with the square-wave bursting of Figure 2*A*. Its slow activation and the slower $[Ca^{2+}]_i$ that inactivates it provide the two variables for a minimal model of a parabolic burster's underlying slow oscillator (see the next section).

Parabolic burst-like features are seen in the 10-Hz oscillations of mammalian thalamic reticular neurons (Figure 2*F*) during the spindle waves of quiet sleep (Steriade et al., 1993). The oscillation depends on a low-threshold calcium current, such as that of triangular bursting. In addition to this current's slow inactivation, there is likely a second slow variable to support the parabolic pattern, e.g., $[Ca^{2+}]_i$ for activating a calcium-dependent potassium current in these cells.

A different kind of burst pattern consists of spike clusters interspersed with epochs of small-amplitude subthreshold oscillations (Figure 2*G*, 2*H*). The envelope of fast events slowly waxes and wanes, forming an approximate spindle or ellipse; hence, the term *elliptic bursting*. Here, the inactive phase is not totally silent, but often shows small oscillations. The frequency of intraburst spiking is comparable to that of the interburst subthreshold oscillations. Only recently has this bursting pattern been reported for mammalian neurons and associated with important functional roles, such as the limbic system's theta rhythm (not shown) and the gamma fast oscillations (approximately 40 Hz) that occur intermittently with increased alertness and focused attention (see Figure 2*H*). Experimental (Llinás, Grace, and Yarom, 1991) and computational (Wang, 1993) studies indicate that the 40-Hz elliptic bursts involve a persistent Na^+ conductance and a specific voltage-dependent transient K^+ conductance.

Some oscillations (Figure 2*I*, 2*J*) depend on the electrical cable properties of neuronal dendrites and intracellular sources of regenerative ion fluxes. The bursting behavior of some pyramidal neurons (Figure 2*I*) in the neocortex (Connors and Gutnick, 1990) and in the hippocampus depends on high-threshold calcium channels located on the distal dendrites, while the faster sodium spikes are generated primarily in the perisomatic region. Computer simulations suggest that a one-compartment description is inadequate and that electrotonically distinct compartments must be explicitly modeled and analyzed (e.g., Traub et al., 1991). Figure 2*J* displays the bursting pattern of a pituitary gonadotropin-releasing cell. While it resembles the square-wave form of Figure 2*A*, here the underlying slow rhythm is generated by a cytoplasmatic second messenger system that leads to nonlinear, time-dependent, calcium fluxes across the endoplasmic reticulum membrane (Stojilkovic and Catt, 1992) and to oscillations in $[Ca^{2+}]_i$.

Bursting Systems Analysis: Fast- and Slow-Phase Space Dynamics

Since different bursters may have qualitatively similar patterns, a qualitative classification should not depend on quantitative properties such as the rhythm's period or its precise biophysical bases. Our general framework involves a *geometrical* analysis of the bursting dynamics for a model's differential equations (Rinzel, 1985, 1987). The model for an isopotential neuron may be written as:

$$\frac{dX}{dt} = F(X, Y) \tag{1}$$

$$\frac{dY}{dt} = G(X, Y) \tag{2}$$

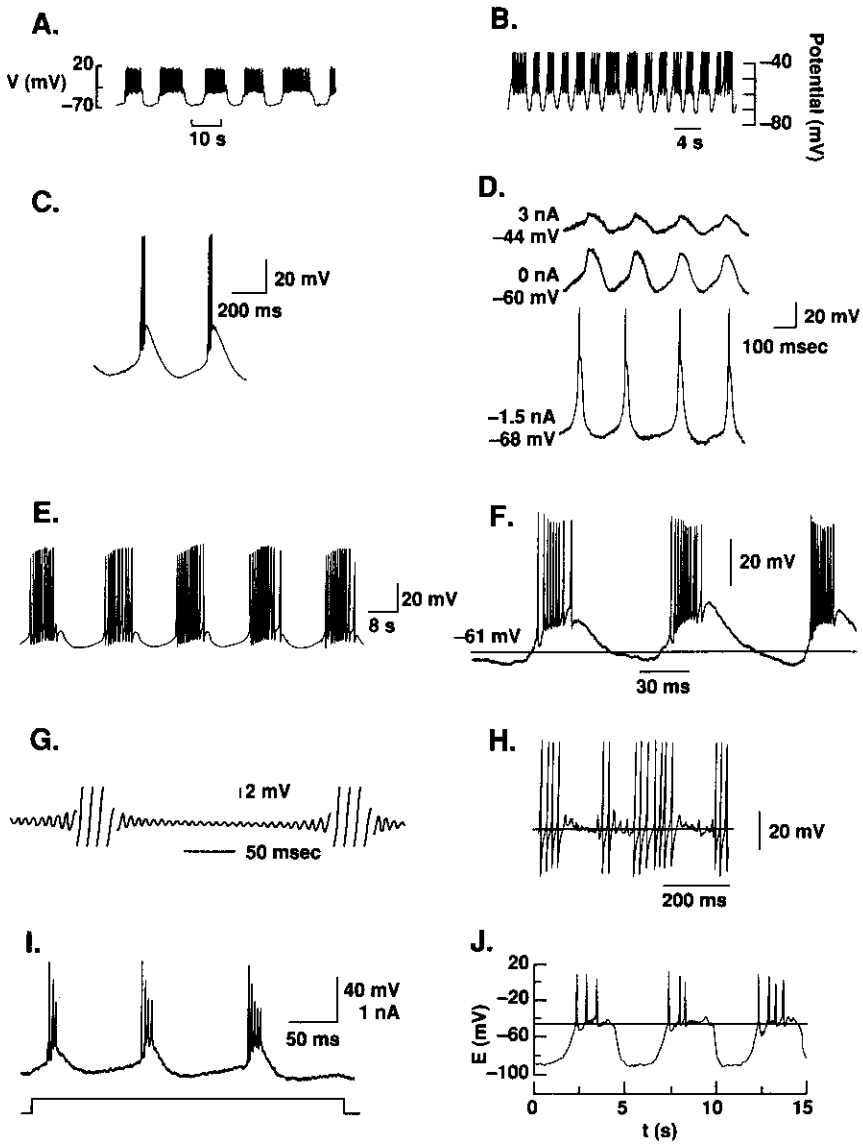

Figure 2. Examples of rhythmic bursting, showing the time courses of membrane potential, with the exception of *G*, which is extracellular voltage. See text for explanations. *A*, Pancreatic β-cell [From Sherman, A., Carroll, P., Santos, R. M., and Atwater, I., 1990, Glucose dose response of pancreatic beta-cells: Experimental and theoretical results, in *Transduction in Biological Systems* (C. Hidalgo et al. Eds.), New York: Plenum, p. 123; reprinted with permission.] *B*, Dopamine-containing neurons in the rat midbrain. (From Johnson, S. W., Seutin, V., and North, R. A., 1992, Burst firing in dopamine neurons induced by *N*-methyl-D-aspartate: Role of electrogenic sodium pump, *Science*, 258:665–667; reprinted with permission. Copyright 1992 by the AAAS.) *C*, Cat thalamocortical relay neuron. (From McCormick, D. A., and Pape, C.-H., 1991, Properties of a hyperpolarization-activated cation current and its role in rhythmic oscillation in thalamic relay neurons, *J. Physiol. Camb.*, 431:291–318; reprinted with permission.) *D*, Guinea pig inferior olivary neuron. (From Benardo, L., and Foster, R. E., 1986, Oscillatory behaviors in inferior olive neurons: Mechanism, modulation, cell aggregates, *Brain Res. Bull.*, 17:773–784; copyright 1986; reprinted with permission from Elsevier Science Ltd.) *E*, *Aplysia* R15 neuron. (From Lotshaw, D. P., Levitan, E. S., and Levitan, I. B., 1986, Fine tuning of neuronal electrical activity: Modulation of several ion channels by intracellular messengers in a single identified nerve cell, *J. Exp. Biol.*, 124:302–322; reprinted with permission of Company of Biologists Ltd.) *F*, Cat thalamic reticular neuron. (From Mulle, C., Madariaga, A., and Deschênes, M., 1986, Morphology and electrophysiological properties of reticularis thalami neurons in cat: In vivo study of a thalamic pacemaker, *J. Neurosci.*, 6:2134–2145; reprinted with permission of the Society for Neuroscience.) *G*, *Sepia* giant axon. (From Arvanitaki, A., 1939, Recherche sur la réponse oscillatoire locale de l'axone géant isolé de *Sepia*, *Arch. Int. Physiol.*, 49:209–256; reprinted with permission.) *H*, Rat thalamic reticular neuron. (From Pinault, D., and Deschênes, M., 1992, Voltage-dependent 40 Hz oscillations in rat reticular thalamic neurons in vivo, *Neuroscience*, 51:245–258; copyright 1992; reprinted with permission from Elsevier Science Ltd.) *I*, Mouse neocortical pyramidal neuron. (From Agmon, A., and Connors, B. W., 1989, Repetitive burst-firing neurons in the deep layers of mouse somatosensory cortex, *Neurosci. Lett.*, 99:137–141; reprinted with permission.) *J*, Rat pituitary gonadotropin-releasing cell. (From Tse, A., and Hille, B., 1993, Role of voltage-gated Na^+ and Ca^{2+} channels in gonadotropin-releasing hormone-induced membrane potential changes in identified rat gonadotropes, *Endocrinology*, 132(4):1475–1481; reprinted with permission. © The Endocrine Society.)

where the vectors X and Y represent the variables with fast and slow time scales, respectively. Typically, the membrane potential is a fast variable, so Equation 1 might be the membrane's current balance equation:

$$C_m \frac{dV}{dt} = -\sum_i I_i + I_{app}$$

The other dynamic variables include the gating variables for specific ionic channels plus relevant second-messenger variables and ionic concentrations. Here, we consider only one or two slow variables Y_k, which might be a slow voltage-dependent gating variable or $[Ca^{2+}]_i$, or both.

The fast- and slow-phase space dissection method (Rinzel, 1985, 1987) exploits the presence of two disparate time scales. For simplicity, suppose there is only one slow variable, Y. One first treats Y as a *control parameter* and considers the dynamics of Equation 1 as a function of Y. The fast subsystem's various behavioral states are then summarized in a bifurcation diagram, plotting response amplitude, for example V, versus Y, as in Figure 1, but where Y (instead of I) is the parameter. When the full system is considered, Y evolves slowly in time according to Equation 2, slowly sweeping through a range of values while the fast subsystem slowly tracks its stable states (*attractors*). For example, an oscillatory state of the fast subsystem corresponds to the repetitive firing of a burst's active phase. During a silent phase, the fast subsystem would be following a pseudo-steady state of hyperpolarized V. To complete the description, one must understand the slow dynamics from Equation 2 to know where on the fast subsystem's bifurcation diagram Y will be increasing or decreasing. When the full system, Equations 1 and 2, is integrated and the resulting burst trajectory is projected onto the (V, Y) plane, it coincides with portions of the bifurcation diagram. Through visualization of this geometrical representation, one can make predictions about the qualitative behavior of bursting and the effects of various parameter changes.

Square-wave bursting. The prototypical fast- and slow-phase plane (Figure 3*A*) was originally developed for the Chay-Keizer model of β-cell bursting (Rinzel, 1985), where $[Ca^{2+}]_i$ was the slow, negative-feedback variable (see the earlier section on neuronal bursting). For the fast-slow dissection, one first constructs the fast subsystem's bifurcation diagram by treating Y as a parameter. This construction yields the Z-shaped curve of steady states. The oscillatory state surrounding the upper branch corresponds to repetitive spiking of an active phase. It terminates by contacting the unstable middle steady-state branch at a homoclinic bifurcation. The Z-curve's lower branch represents a stable steady state of hyperpolarization as tracked during a burst's silent phase. In an intermediate range of Y values, there is bistability of the depolarized oscillation and the hyperpolarized steady state.

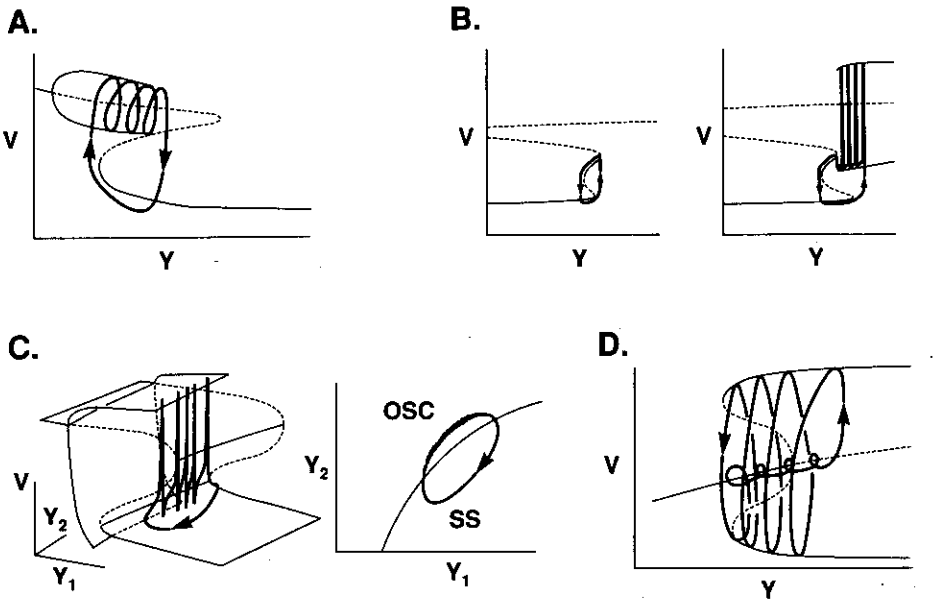

Figure 3. Fast- and slow-phase plot of bursting dynamics. The variable Y is a slow variable (there are two slow variables Y_1 and Y_2 in part *C*). In each case, the bifurcation diagram is computed for the fast subsystem, with Y treated as a parameter, and plotted in terms of the membrane potential (V) behavior as a function of Y. The solid curve shows stable and the dashed curve unstable branches. The oscillatory state of repetitive firing is represented by its maximum and minimum of V (cf. Figure 1). The heavy curves with arrows are bursting trajectories of the full system plotted on the (V, Y) plane or the (V, Y_1, Y_2) space. *A*, Square-wave bursting is based on a bistability of a steady state and a repetitive firing state in the fast subsystem and periodic switching between the two, induced by the slow-variable dynamics. *B*, Triangular bursting has a similar phase plot as in part *A*, but the fast subsystem's steady-state curve is quintic rather than cubic, with two branches of stable steady states. Depending on whether the stable repetitive firing state overlaps with the lowermost steady-state branch, oscillations of the full system may be either purely subthreshold (left panel) or bursting (right panel). For simplicity, the repetitive firing state is shown only on the right panel, not on the left panel. *C*, Parabolic bursting is generated by an oscillation in a two-variable (Y_1 and Y_2) slow subsystem (right panel) that induces smooth periodic switching between a steady state (SS) and a repetitive spiking state (OSC) (which do not overlap) of the fast subsystem. *D*, Elliptic bursting involves a subcritical Hopf bifurcation in the fast subsystem. Bursting involves slow switching between a steady state and a repetitive firing state that are bistable in the fast subsystem. The silent phase exhibits damped or growing small oscillations as its trajectory passes through the Hopf bifurcation point. (Parts *A* and *C–D* are adapted from Rinzel, 1987; Part *B* from Rush, M., and Rinzel J., 1994, *Biol. Cybern.*, 71:281–291.)

Next, Y is allowed to vary according to its kinetics. Bursting occurs if the slow kinetics dictate that Y increases (decreases) when the fast spike-generating subsystem is in its upper (lower) state, where the voltage-dependent channels are (are not) activated. The slow Y modulation induces abrupt switching between the two coexisting states, and thus temporal alternation occurs between a train of spikes and a resting phase, as seen in Figure 2*A*.

Triangular bursting. Figure 3*B* shows fast- and slow-phase planes associated with triangular bursting. A minimal model has one slow variable, and its fast subsystem has regimes of bistability, as with square waves. Here, however, the steady-state curve has five branches composed of *two* S-shaped portions in different V ranges. These S-curves correspond to the two sets of regenerative currents active in the subthreshold voltage ranges, such as in thalamic relay or inferior olivary cells. The depolarized oscillatory state (repetitive spiking) joins the middle steady-state branch at its right knee (a saddle-node homoclinic bifurcation). Different oscillation patterns occur depending on whether the right knee of the lower S extends rightward beyond that of the right knee of the upper S. Otherwise (see Figure 3*B*, left), a slow subthreshold oscillation without fast spikes may occur. The alternative case (see Figure 3*B*, right) corresponds to more intense hyperpolarizing input, when triangular bursting arises (see Figure 2*D*). The term *triangular* refers to the gradually falling V time course of the active phase, related to the middle branch's steep slope (see Figure 3*B*).

Parabolic bursting. This bursting type has a smooth, underlying slow-subthreshold wave. Its generation requires at least two slow variables, one for positive feedback and the other for negative feedback. The minimal fast- and slow-phase plot has three dimensions: V and the two slow variables (Figure 3*C*, originally constructed for a model of the *Aplysia* R15 neuron; see Rinzel, 1987). Steady states of the fast subsystem are now represented by a *Z-surface*. Similarly, a surface describes the fast oscillatory (repetitive spiking) attractors. These periodic solutions disappear through homoclinic bifurcation as they contact the Z-surface precisely at its lower knee, forming a saddle-node coalescence (see Figure 1). Here, the fast subsystem is monostable. The slow-variable-phase plane is divided into two nonoverlapping regions: one for the resting steady state and the other for the repetitive spiking regime of the fast subsystem.

When the slow variables are allowed to vary, an oscillation may occur in this two-variable slow system (see Figure 3*C*, right). If the slow oscillatory trajectory visits both of the fast subsystem's regimes, bursting occurs, with repetitive smooth switching between the resting and spiking states. As a burst begins and ends, its trajectory crosses a homoclinic bifurcation of the fast subsystem and spike frequency drops dramatically; hence, the parabolic nature.

Elliptic bursting. A minimal model has only one slow variable (Figure 3*D*, originally constructed for a modified FitzHugh-type model; see Rinzel, 1987). The fast subsystem has bistability because of a *subcritical* Hopf bifurcation (see Figure 1) of periodic solutions from a monotonic steady-state curve. As with square waves, during bursting, the full system operates in the (V, Y) regime of bistability, repetitively switching between the steady state and the spiking state. A distinguishing feature, however, is that the silent phase, when the fast subsystem operates near its steady state, is no longer truly silent: it can display small oscillations which damp and then grow as the trajectory slowly passes through the Hopf bifurcation point, where the steady state is a spiral-type fixed point.

Complex bursting. The theoretical study of certain bursting types (see Figure 2*I*, 2*J*) is relatively recent, and mathematical understanding of their mechanisms is just emerging. For analyzing the case of Figure 2*I*, one requires a minimal model of at least two electrotonically separated compartments. Electrical coupling might introduce another, possibly intermediate, time scale. As for Figure 2*J*, one must take into account the interaction between second-messenger-mediated calcium fluxes from intracellular pools and voltage-dependent plasma membrane calcium currents.

The classification discussed here is based on various fast- and slow-phase plots. Although consistent with some of the waveform phenomenology, the two may sometimes disagree. For instance, a system with the fast- and slow-phase plot of Figure 3*C* may burst with a slow wave that is less sinusoidal and more rectangular if one slow variable is much slower than the other. However, in contrast to a square-wave burster (see Figures 2*A* and 3*A*), its slow wave may persist, even with the fast action potentials blocked.

Discussion

We have reviewed various neuronal bursting oscillations and, by using notions and analytic tools from the mathematics of dynamical systems, we discussed how these bursting patterns might be theoretically described and classified. Our examples are minimal for these categories. Indeed, one can imagine subcategories based on differences in the fast subsystem's bifurcation diagram. In summary, bursting in a single-compartment model typically involves some slow processes which induce repetitive switching between a relatively quiescent state and an active state of repetitive spiking of a faster system. In the cases of square-wave, triangular, and elliptic bursting, one slow variable is sufficient, and the fast subsystem must be bistable. In the case of parabolic bursting, bistability in the fast subsystem is not necessary, and two slow variables are required.

The geometrical analysis by fast and slow dissection illustrates how novel and powerful theoretical approaches can emerge from fruitful interactions between neurobiology and the science of dynamical systems. Possible extensions might consider cable-like distributed systems with local burst-generating dynamics, systems with many slow variables, or systems with complicated bifurcation diagrams, perhaps involving chaotic attractors. One can expect that dynamical systems methods, including fast and slow dissection, may also play a role in our understanding of neural networks with many synaptically coupled neurons, as long as there are disparate time scales in the system.

Road Map: Biological Neurons
Background: Dynamics and Bifurcation of Neural Networks; Ion Channels: Keys to Neuronal Specialization
Related Reading: Half-Center Oscillators Underlying Rhythmic Movements; Thalamocortical Oscillations in Sleep and Wakefulness

References

Adams, W. B., and Benson, J. A., 1985, The generation and modulation of endogenous rhythmicity in the *Aplysia* bursting pacemaker neurone R15, *Prog. Biophys. Mol. Biol.*, 46:1–49. ◆

Arvanitaki, A., 1939, *Les Variations graduées de la polarization des systèmes excitables*, Paris: Hermann. ◆

Connors, B. W., and Gutnick, M. J., 1990, Intrinsic firing patterns of diverse neocortical neurons, *Trends Neurosci.*, 13:99–104. ◆

Cook, L. D., Satin, L. S., and Hopkins, W. F., 1991, Pancreatic B cells are bursting, but how? *Trends Neurosci.*, 14:411–414. ◆

FitzHugh, R., 1961, Impulses and physiological states in models of nerve membrane, *Biophys. J.*, 1:445–466.

Hodgkin, A. L., 1948, The local electric changes associated with repetitive action in a non-medullated axon, *J. Physiol. (Lond.)*, 107:165–181.

Hodgkin, A. L., and Huxley, A. F., 1952, A quantitative description of membrane current and its application to conduction and excitation in nerve, *J. Physiol. (Lond.)*, 117:500–544.

Llinás, R., 1988, The intrinsic electrophysiological properties of mammalian neurons: Insights into central nervous system function, *Science*, 242:1654–1664. ◆

Llinás, R. R., Grace, T., and Yarom, Y., 1991, *In vitro* neurons in mammalian cortical layer 4 exhibit intrinsic oscillatory activity in the 10- to 50 Hz frequency range, *Proc. Natl. Acad. Sci. USA*, 88:897–901.

Llinás, R. R., and Yarom, Y., 1986, Oscillatory properties of guinea-pig inferior olivary neurones and their pharmacological modulation: An *in vitro* study, *J. Physiol. (Lond.)*, 376:163–182.

Rinzel, J., 1985, Bursting oscillations in an excitable membrane model, in *Ordinary and Partial Differential Equations: Proceedings of the 8th Dundee Conference* (B. D. Sleeman and R. J. Jarvis, Eds.), Lecture Notes in Mathematics, 1151, New York: Springer, 304–316.

Rinzel, J., 1987, A formal classification of bursting mechanisms in excitable systems, in *Proceedings of the International Congress of Mathematicians* (A. M. Gleason, Ed.), Providence, RI: American Mathematical Society, pp. 1578–1594.

Rinzel, J., and Ermentrout, G. B., 1989, Analysis of neural excitability and oscillations, in *Methods in Neuronal Modeling: From Synapses to Networks* (C. Koch and I. Segev, Eds.), Cambridge, MA: MIT Press, 135–169. ◆

Steriade, M., McCormick, D. A., and Sejnowski, T. J., 1993, Thalamocortical oscillations in the sleep and aroused brain, *Science*, 262: 679–685. ◆

Stojilkovic, S. S., and Catt, K. J., 1992: Calcium oscillations in anterior pituitary cells, *Endocr. Rev.*, 13:256–280. ◆

Traub, R., Wong, R., Miles, R., and Michelson, H., 1991, A model of a CA3 hippocampal pyramidal neuron incorporating voltage-clamp data on intrinsic conductances, *J. Neurophysiol.*, 66:635–649.

Wang, X.-J., 1993, Ionic basis for intrinsic 40 Hz neuronal oscillations, *Neuroreport*, 5:221–224.